Simulating the Role of Surface Forcing on Observed Multidecadal Upper-Ocean Salinity Changes

VÉRONIQUE LAGO,*,+ SUSAN E. WIJFFELS,* PAUL J. DURACK,*,# JOHN A. CHURCH,*
NATHANIEL L. BINDOFF,*,+,@ AND SIMON J. MARSLAND&

* *Centre for Australian Weather and Climate Research, CSIRO Oceans and Atmosphere, Hobart, Tasmania, Australia*
+ *Institute for Marine and Antarctic Studies, University of Tasmania, Hobart, Tasmania, Australia*
# *Program for Climate Model Diagnosis and Intercomparison, Lawrence Livermore National Laboratory, Livermore, California*
@ *Antarctic Climate and Ecosystems Cooperative Research Centre, Hobart, Tasmania, Australia*
& *Centre for Australian Weather and Climate Research, CSIRO Oceans and Atmosphere Flagship, Aspendale, Victoria, Australia*

(Manuscript received 23 July 2015, in final form 9 November 2015)

ABSTRACT

The ocean's surface salinity field has changed over the observed record, driven by an intensification of the water cycle in response to global warming. However, the origin and causes of the coincident subsurface salinity changes are not fully understood. The relationship between imposed surface salinity and temperature changes and their corresponding subsurface changes is investigated using idealized ocean model experiments. The ocean's surface has warmed by about 0.5°C $(50\,\mathrm{yr})^{-1}$ while the surface salinity pattern has amplified by about 8% per 50 years. The idealized experiments are constructed for a 50-yr period, allowing a qualitative comparison to the observed salinity and temperature changes previously reported. The comparison suggests that changes in both modeled surface salinity and temperature are required to replicate the three-dimensional pattern of observed salinity change. The results also show that the effects of surface changes in temperature and salinity act linearly on the changes in subsurface salinity. Surface salinity pattern amplification appears to be the leading driver of subsurface salinity change on depth surfaces; however, surface warming is also required to replicate the observed patterns of change on density surfaces. This is the result of isopycnal migration modified by the ocean surface warming, which produces significant salinity changes on density surfaces.

1. Introduction

Previous works have reported coherent patterns of multidecadal salinity changes within the oceans (Freeland et al. 1997; Wong et al. 1999, 2001; Dickson et al. 2002; Curry et al. 2003; Boyer et al. 2005; Johnson and Lyman 2007; Gordon and Giulivi 2008; Cravatte et al. 2009; Hosoda et al. 2009; Roemmich and Gilson 2009; von Schuckmann et al. 2009; Durack and Wijffels 2010; Helm et al. 2010; Kouketsu et al. 2010; Durack et al. 2013; Skliris et al. 2014). However, the cause of these salinity changes is not fully understood. Ocean salinity is linked to the global water cycle primarily through evaporation-minus-precipitation ($E - P$) fluxes along with terrestrial runoff (Schanze et al. 2010), which together define the spatial pattern of salinity at the ocean surface. It has been hypothesized that water cycle amplification (the enhancement of the water fluxes at the surface of the ocean—e.g., $E - P$) is a major driver of the subsurface salinity changes (Bindoff and McDougall 1994, Wong et al. 1999, 2001; Curry et al. 2003; Hosoda et al. 2009; Helm et al. 2010; Durack et al. 2012; Terray et al. 2012). The ocean's dynamic nature ensures that along with $E - P$, ocean temperature, circulation, and mixing changes also play a role in driving changes to the ocean's salinity field.

The water cycle has likely amplified in response to observed global warming (Hartmann et al. 2013; Rhein et al. 2013; Hegerl et al. 2014) as a result of the increased capacity of the warmer atmosphere to hold water vapor following the Clausius–Clapeyron relation (Held and

Corresponding author address: Véronique Lago, CSIRO Marine and Atmospheric Research, GPO Box 1538, Hobart, TAS 7001, Australia.
E-mail: veronique.lago@csiro.au

DOI: 10.1175/JCLI-D-15-0519.1

Soden 2006). However, quantifying water cycle changes from the poorly constrained, highly variable and episodic precipitation or surface fluxes is difficult. Observed analyses of global ocean salinity change potentially provide insight into water cycle change. In climate models, Durack et al. (2012) demonstrated that in those with a surface warming, a stronger water cycle amplifies the ocean's surface salinity pattern such that regions of the oceans that are saltier than the global mean become saltier over time and regions that are fresher than the global mean become fresher, consistent with observed changes (Durack et al. 2012; Rhein et al. 2013).

As noted above, there are many studies that have investigated long-term changes to both global and regional salinity patterns. Durack and Wijffels (2010) compiled 59 years (1950–2008) of global ocean salinity observations and reported the long-term salinity change patterns. Their analysis suggested that surface-forced salinity changes, along with surface and subsurface temperature changes, are responsible for the observed trends of subsurface salinity changes. Following previous studies (Bindoff and McDougall 1994; Wong et al. 1999, 2001; Curry et al. 2003), Durack and Wijffels (2010) analyzed the pattern of salinity change on density surfaces and found features that were repeated independently in each ocean basin. The subsurface salinity changes propagate into the interior along isopycnals driven by subtropical subduction.

During the 1950–2000 period, the near-surface ocean has warmed by about 0.5°C, including the subtropical gyres, but with less warming in the high latitudes (Rhein et al. 2013). As a result of this broad-scale warming in the subtropics, the location of the surface isopycnal outcrops has been shifting poleward by about 50–100 km, driving an outcrop migration through the climatological mean surface salinity field, which to first order is stationary (Durack and Wijffels 2010). The poleward shift of isopycnals results in a predictable pattern of change of the salinity injected into the oceans interior by normal wind-driven subduction (Drijfhout et al. 2013). Isopycnals that outcrop equatorward of the subtropical salinity horizontal maximum migrate poleward into a saltier surface regime and thus experience a surface salinity increase, while those that outcrop poleward of the horizontal maximum migrate into a fresher regime and experience a surface freshening. Durack and Wijffels (2010) show the connection between the salinity changes on isopycnals and the corresponding surface salinity in their Figs. 9 and 10. This yields a pattern of change that is almost orthogonal to the mean salinity pattern (in density space)—that is, with the strongest change signal appearing in the gradient regions of the climatological mean salinity (Durack and Wijffels 2010). At the surface salinity maximum regions, the subsurface salinity trend changes sign as the migrating outcrop passes from a surface salinity increase to a decrease and vice versa for the surface salinity minimum.

While the warming-driven outcrop migration process appears to be at work (Durack and Wijffels 2010), there is also strong observational and model evidence for the intensification of the surface salinity pattern due to the amplified water cycle (Helm et al. 2010; Durack et al. 2012; Hegerl et al. 2014). Hence, the resolved changes to subsurface ocean salinity are likely due to a combination of these surface-forced processes. Additionally, coincident multidecadal changes to ocean mixing and circulation are possible. The current observational coverage, however, means little can be confidently assessed about such changes to the general circulation (Rhein et al. 2013).

Here, we aim to understand the drivers of the observed subsurface salinity and water mass changes and in particular understand whether the processes of outcrop migration and/or surface salinity pattern amplification are indeed the primary drivers. We use a global ocean model to evaluate the relative contribution of these separate surface forcing terms. In particular, we investigate the role of surface salinity pattern amplification and surface temperature increases by undertaking four idealized simulations (control, changed surface temperature, changed surface salinity, and changes in both surface temperature and salinity). We use this idealized decomposition to assess the mechanisms that are driving the subsurface changes assessed in both depth and isopycnal (water mass) frameworks. The results are compared with observations (Durack and Wijffels 2010).

This paper is the first in a series of three that decomposes the role of changes at the surface of the ocean to the observed changes in the ocean interior. In this paper, we focus on the impact of the surface temperature increase and salinity pattern amplification to the changes in salinity at the subsurface. In the second paper, we assess the impact of the surface temperature increase and salinity pattern amplification to the changes in temperature in the ocean interior. In the third paper, we will focus on the changes in salinity and temperature in the ocean interior due to changes in the wind patterns.

2. Methods

The model used in this study is the Australian Community Climate and Earth System Simulator Ocean Model (ACCESS-OM; Bi et al. 2013). It is a coupled global ocean and sea ice model that combines the

Modular Ocean Model version 4.1 (MOM4p1; Griffies 2009), the data-driven atmospheric model (MATM), and the Los Alamos National Laboratory Sea Ice Model version 4.1 (CICE4.1; Hunke and Lipscomb 2010). These submodels exchange information through numerical coupling with OASIS3 (Valcke 2006).

The grid has a resolution of 1° in the zonal direction (between ~23 km at 78°S and ~111 km at the equator). The meridional resolution varies from ¼° at 78°S (~27 km) to 1° at 30°S (~111 km) with equatorial refinement to ⅓° between 10°S and 10°N (~37 km). There are 50 levels of varying thickness in the vertical direction between 0 and 6000 m. The vertical layers are thinner at the surface (10 m) and thicker at depth (up to 333 m thick). The topography is approximated by a partial cell method. The tracers and velocity are evaluated on a common Arakawa B grid (Arakawa and Lamb 1977) for both ocean and sea ice models.

The normal year forcing version of the Co-ordinated Ocean–Ice Reference Experiments (CORE) dataset from Large and Yeager (2004, 2009) is imposed on the ocean and ice submodels through the MATM, using the CORE experimental design as outlined in Griffies et al. (2009). The CORE forcings and bulk formulas used are version 2 (COREv2) as defined in Large and Yeager (2004, 2009). The 500-yr ocean–ice model spinup simulation was qualitatively similar to other CORE models (see Griffies et al. 2009) and provided a stable state for the commencement of the experiments considered herein. As for most models of its kind, some deep water mass adjustment continues after spinup, but this will be explicitly dealt with below.

Bi et al. (2013) assessed in detail the state of the ACCESS-OM model after a 500-yr spinup, finding that the model has a realistic global ocean circulation and property field, with most major upper-ocean water masses represented fairly well. As for many coarse-resolution Z grid models, water mass tongues are eroded too quickly and do not penetrate as far equatorward as in the observed oceans (Sloyan and Kamenkovitch 2007) and the main thermocline is too deep and too thick. The Indonesian Throughflow (ITF) is also not well defined. However, overall, wind-driven subduction and the subtropical and equatorial circulation systems appear to be well simulated (Bi et al. 2013).

To explore how surface changes are transferred to the ocean interior over 50 years, we carried out four idealized forcing experiments (Table 1). First, after the 500-yr spinup, a 50-yr control run was performed where we continue to force the model with the COREv2 normal year wind stress used in the spinup but strongly control surface temperature and salinity by imposing 6-hourly restoring to a seasonal climatology based on the last year of the spinup. This allows us to quantify the small but continuing residual drift of the deep water masses in this model. A second 50-yr experiment (referred to as ΔT here) is identical to the control except that surface temperature is linearly warmed with time to achieve a 0.5°C rise between 60°N and 55°S (Fig. 1a), while surface salinity is restored to the mean seasonal cycle every 6 h. The third experiment (ΔS) is identical to the control except that temperature is restored to the mean seasonal cycle every 6 h, but the mean salinity pattern is amplified over 50 years by 8% (Fig. 1b). By keeping the surface forcing condition of COREv2, we ensure that the only changed variable in the experiments is the surface temperature or salinity. The fourth and final experiment ($\Delta T\Delta S$) imposes the temperature warming and salinity pattern amplification at the same time. This will allow us to diagnose any nonlinear interactions of the surface forcing. For all experiments the wind stresses are identical. Table 1 summarizes the experiments.

TABLE 1. List of experiment nomenclature and corresponding imposed ocean surface conditions.

Experiment name	Control (C)	Temperature (ΔT)	Salinity (ΔS)	Combined ($\Delta T\Delta S$)
Temperature uniform increase (°C)	0	0.5	0	0.5
Salinity pattern amplification (%)	0	0	8	8

In ΔT, we are imposing an idealized version of the observed surface warming from observations for the period 1950–2000. The latitude limits chosen for the warmed portion of the ocean surface are based on the zonally averaged observations of Durack and Wijffels (2010), but they also allow us to avoid strong interactions with the model's sea ice component (Fig. 1c). While changes in the polar regions of our results need to be viewed with caution, our primary focus is on the actively subducting subtropical/equatorial circulation and thermocline water masses. In ΔS, the anomaly imposed on the restoring fields is proportional to the local difference from the global area-weighted mean for that month and is linearly increased up to 8% at the end of the 50-yr period (Fig. 1a). The monthly global average surface salinity used for calculating the imposed anomaly varies between 34.00 in August and 34.21 in April, calculated as the global mean from the last year of the spinup to ensure continuity and to take into consideration the intra-annual variations.

Given the strong surface restoring we apply, the model surface fields respond as expected, as an idealized representation of the observed surface changes (Fig. 1).

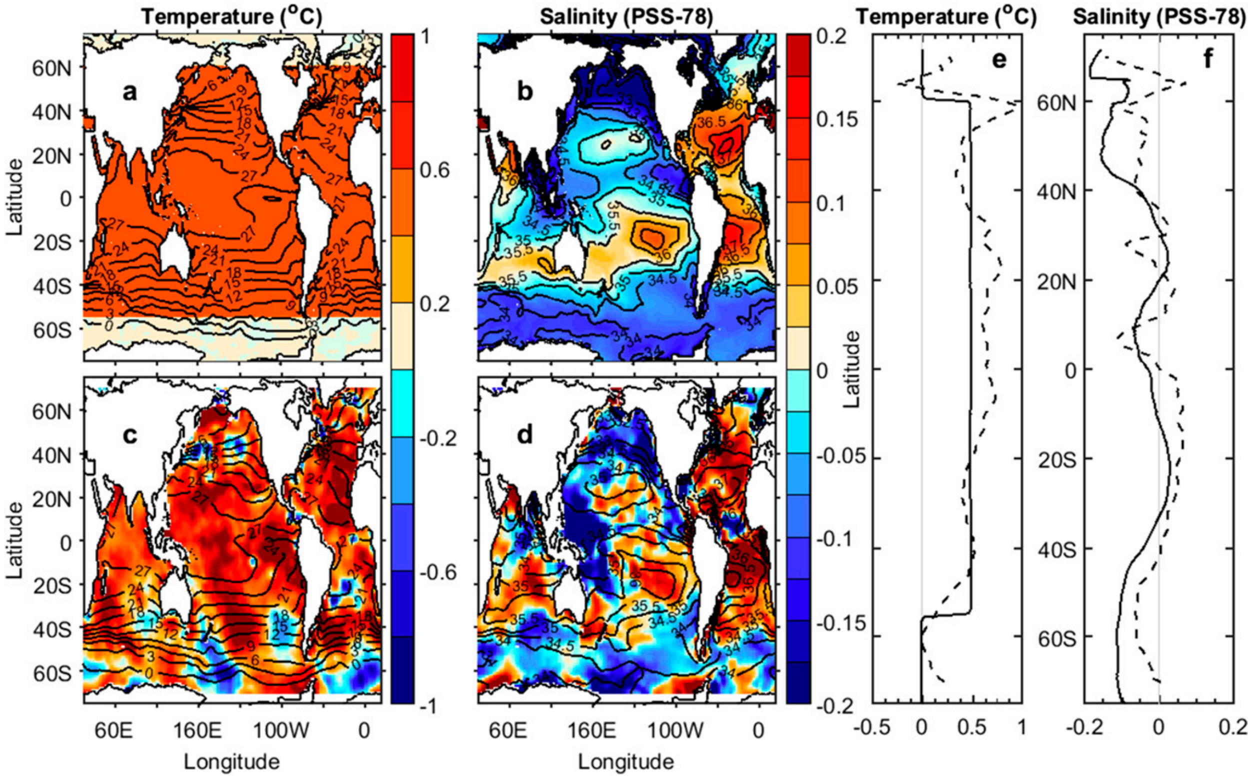

FIG. 1. (a),(c) Temperature and (b),(d) salinity changes for a 50-yr period. (top) Changes imposed in the model and (bottom) the observed changes for the period 1950–2000. The black contours are the mean field every 3°C and every 0.5 PSS-78 for the temperature and salinity respectively. (right) The global zonally averaged (e) temperature and (f) salinity changes from the experiments (solid line) and observations (dashed line).

The surface fields reproduce the uniform warming and salinity pattern amplification seen in the observations. However, these experiments are idealized and are thus not an exact representation of the full complexity of the temporal and regional variations in surface changes observed over the last 50 years. There are spatial variations in the observed surface warming with areas with stronger warming than the 0.5°C mean and areas with cooling in the high latitudes; these spatial variations are not simulated in the idealized experiments (Fig. 1c). However, on average the warming we impose is consistent with the observations (Fig. 1e). In the Atlantic, there is stronger positive salinity change than in our idealized experiment as well as a freshening region at the equator (Figs. 1b,d). In the North Pacific, there are more regions of positive salinity trend than in the experiment, and the overall freshening is stronger in our experiment than in the observations. Notably, the surface salinity is not amplified as much in the Atlantic and the other high-salinity regions in the model. There are also observed regions of positive salinity trends in the high-latitude Southern Ocean that are not simulated, although the observations are sparse and uncertain in that region. Overall, the global zonally averaged salinity changes in the model are fresher than in the observations (Fig. 1f). These differences between the imposed changes and those observed have to be taken into account when comparing our subsurface modeled changes with the observations (Durack and Wijffels 2010).

We present analyses of salinity changes zonally averaged in basins, which are defined by the area masks shown in Fig. 2. These have been chosen to exclude marginal seas and are identical to those used in the observational analysis of Durack and Wijffels (2010). All salinity results presented are using the Practical Salinity Scale of 1978 (PSS-78) and temperatures are in °C.

The control experiment provides information about remaining drift in the model during the 50 years of the experiments (Fig. 3). The salinity trends are small (less than about ± 0.025) compared to the trends observed and produced in our experiments. The control drift is positive almost everywhere, except for the Indian Ocean deeper than 500 m and denser than 27 kg m^{-3}. The trends from the control experiment are subtracted from all the results presented on a gridpoint basis.

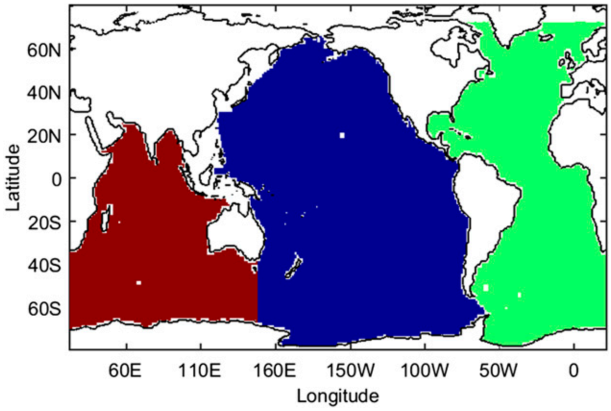

FIG. 2. Definition of the spatial domain of the Atlantic (blue), Pacific (red), and Indian (green) Oceans for zonal averaging used in this study.

The surface restoring in our idealized experiment create long-term change in the heat and salt content of the global ocean. The total heat content change in ΔT from the surface to 2000 m, which are the depths at which we compare our results, is $\sim 20 \times 10^{22}$ J. This is consistent with changes in heat content reported in previous studies for a similar time period (Levitus et al. 2005, 2012). Perhaps more surprisingly, ΔS also induces change in the heat content of the top 2000 m of the same amplitude, with $\sim 21 \times 10^{22}$ J. In $\Delta T \Delta S$, the total heat content change from the surface to 2000 m is $\sim 41 \times 10^{22}$ J. That is more than observed, which is due partly to the absence of the cooling effect from changes in the wind pattern and to the idealized nature of these experiments. The changes in the heat content and temperature induced by the changes in the surface salinity in ΔS and wind pattern will be discussed in detail in the second and third paper of this series of three. The changes in heat content from these experiments also reach deeper than 2000 m, but most of the heat remains within this upper layer. The change in the global mean salinity for the top 2000 m is $\sim 10^{-4}$ PSS-78 in all experiments as there are no other sources of salt than that through the surface layer, which we restore either to a fixed field or to an amplification around the global surface mean salinity.

3. Results

We first examine the impact of the imposed surface changes on the locations of isopycnal outcrops in the model (Fig. 4). In ΔT, the outcrops shift poleward over

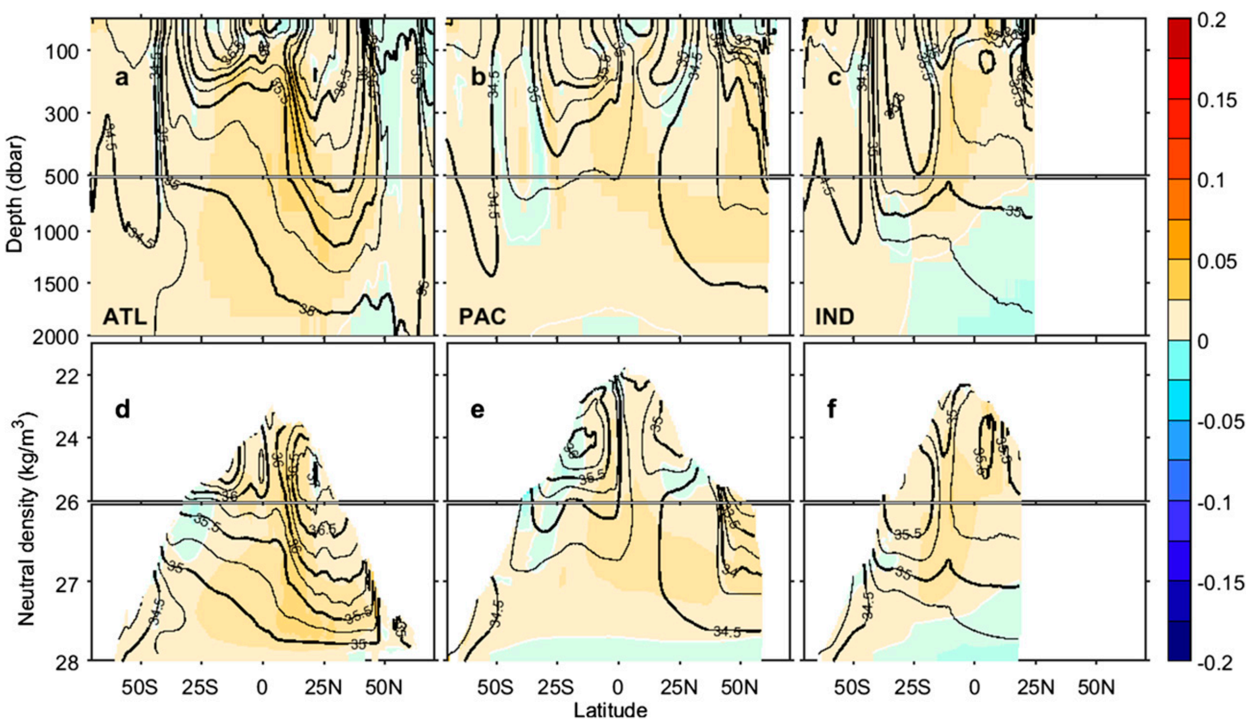

FIG. 3. Zonally averaged salinity changes [PSS-78 (50 yr)$^{-1}$] in the control experiment for the (a),(d) Atlantic, (b),(e) Pacific, and (c),(f) Indian Oceans. (top) Depth space and (bottom) density space are shown. The white contours are the salinity trend every 0.1 PSS-78. The black contours are the mean salinity every 0.5 PSS-78 (thick lines) and 0.25 PSS-78 (thin lines). The scale is the same as that used in subsequent plots for comparison.

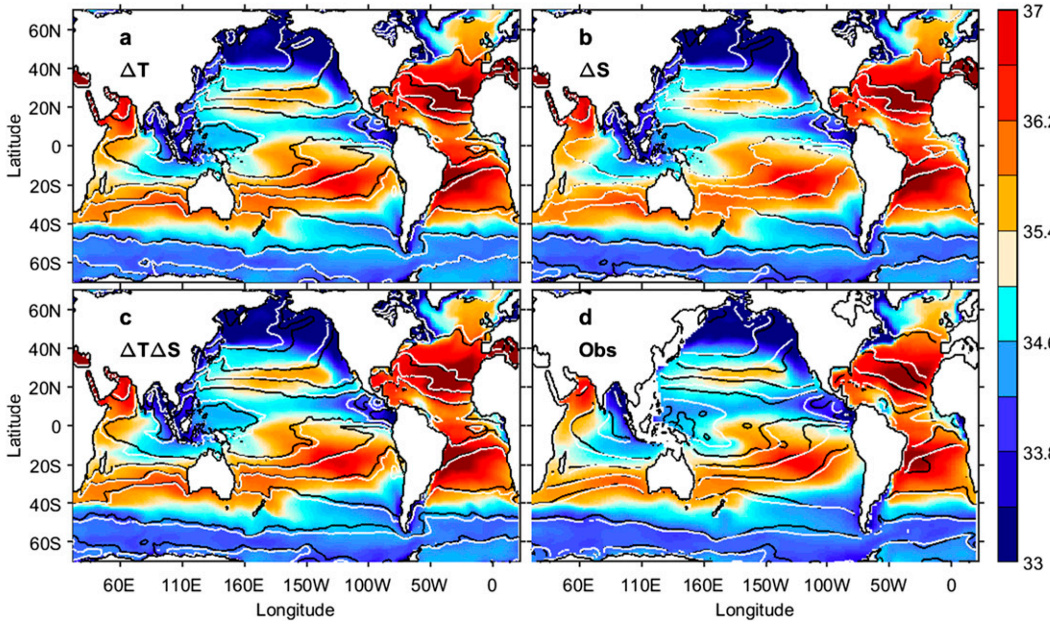

FIG. 4. Density outcrop at the beginning (black) and at the end (white) for (a) ΔT, (b) ΔS, (c) $\Delta T\Delta S$, and (d) the observations. The color pattern shows the mean salinity field (PSS-78).

the 50 years, which is comparable to or sometimes slightly smaller than that analyzed from observations (Durack and Wijffels 2010); this is consistent with the observed warming being mostly less than the imposed warming (Fig. 1e). Near the poles, where no warming is imposed, outcrops do not move, as expected. In ΔS, the density outcrop locations show very little change over the 50 years, except for the high-latitude regions where at low temperatures salinity plays the dominant role in changes of density and we see some poleward shift. Similarly, freshening in the western equatorial Pacific drives outcrops eastward and poleward. Thus, in these regions the salinity changes enhance the isopycnal migration induced by ΔT (Fig. 4).

a. Changes in depth surfaces

When viewed as a zonal average on depth surfaces in the three ocean basins, most of the observed salinity changes are qualitatively reproduced in ΔS (Fig. 5) and, as in the observations, represent a strengthening of the mean salinity pattern (though this effect is stronger near the surface). Thus, we see the shallow fresh tropical salinity minima getting fresher in every basin, the salinity maxima tongues in the subtropics getting saltier, and the salinity minima associated with the Antarctic Intermediate Water (AAIW) in the Southern Hemisphere gyres getting fresher. The surface polar oceans freshen in all basins, as observed.

We note that some of the model water mass biases can be detected in the mean salinity field. For instance, compared to the observations, the mean AAIW minima are poorly formed in the model's Southern Hemisphere gyres and do not form a distinct equatorward-reaching tongue (Sloyan and Kamenkovich 2007). Thus, the freshening tongue of the AAIW is not as well defined. The denser salty Red Sea water is weak in the model's north Indian Ocean, as is the associated salinity maximum. The fresh thermocline plume of the ITF is too weak in the model. In general, most water mass extrema are weaker in the model mean compared to the observations, hinting at too much diffusion given the exactitude of the surface property fields (Fig. 3).

In ΔT, salinity changes at depth are much smaller than in ΔS, which is consistent with the idea that the circulation pathways are largely unchanged since the wind forcing is fixed, and the injection of salinity into the thermocline is largely unchanged. There is a freshening pattern in the midlatitudes of the Southern Hemisphere between 400 and 1000 m in each ocean basin. This feature is also present in the observations as a freshening between the surface and 1500 m. The freshening from the surface down to 1000–1500 m is reproduced in the ΔS only, but the deeper part of this freshening is amplified with ΔT and thus more realistic in $\Delta T\Delta S$. There is also a mid-depth and deep freshening in the midlatitude North Atlantic induced by the surface temperature increase. At the same location, the water is getting saltier in ΔS. The total salinity increase in the mid-depth North Atlantic in $\Delta T\Delta S$ is reduced by the freshening induced by

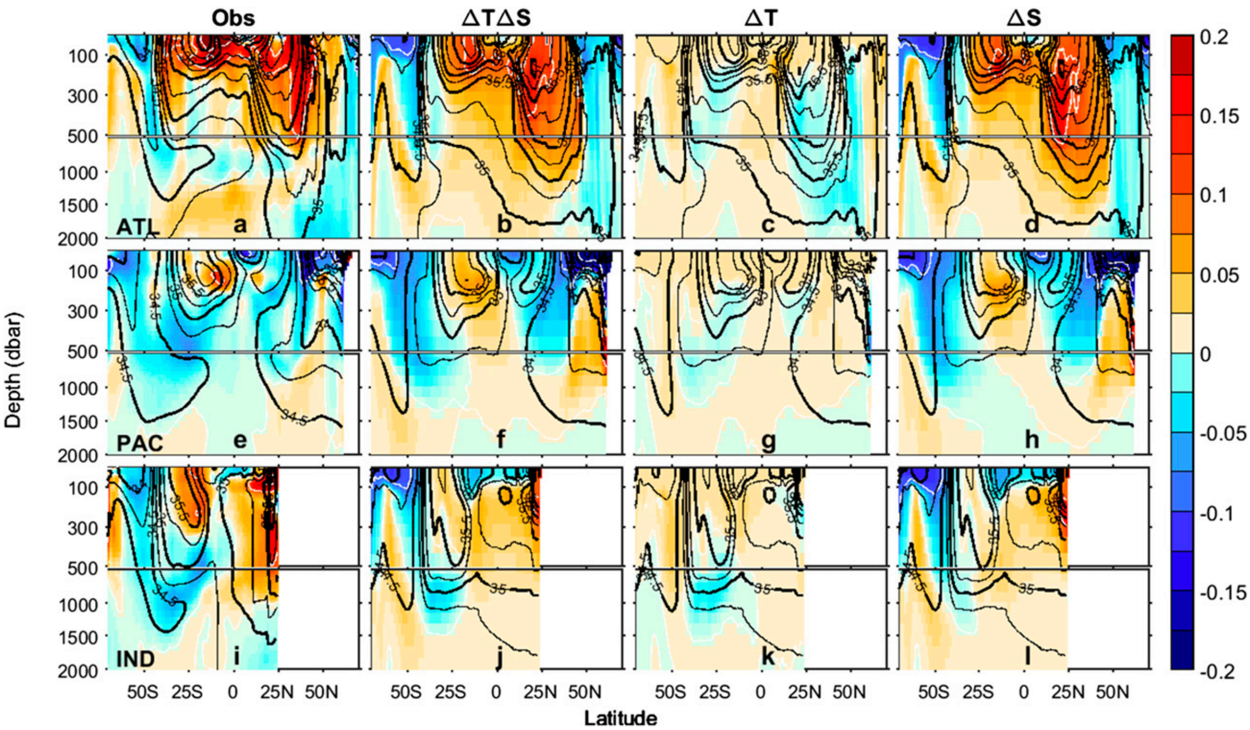

FIG. 5. Zonally averaged salinity changes [PSS-78 $(50\,\mathrm{yr})^{-1}$] in the (a)–(d) Atlantic, (e)–(h) Pacific, and (i)–(l) Indian Oceans. (left to right) Observations, $\Delta T\Delta S$, ΔT, and ΔS. The white contours are the salinity trend every 0.1 PSS-78. The black contours are the mean salinity every 0.5 PSS-78 (thick lines) and 0.25 PSS-78 (thin lines).

the surface temperature increase and thus closer to the observed trend.

Most other effects of observed salinity changes on depth surfaces are reproduced mainly by ΔS. Where the surface becomes fresher or saltier, changes are transferred to the subsurface through subduction. This suggests that most of the subsurface salinity changes on depth surfaces are driven by surface salinity pattern amplification. However, some small contributions from ΔT under the gyres add to a more realistic result in $\Delta T\Delta S$.

b. Water mass changes

To examine how water masses respond to the idealized forcings we examine changes on density surfaces. As there is little change in the salinity field in depth space with ΔT and all surface forcings are fixed except for an increase in surface temperature, changes in salinity with ΔT are driven solely by migration of isopycnals through the mean salinity field. Likewise, in ΔS, all fields being constant except for the surface salinity, changes in the salinity field on isopycnals are mainly driven by the penetration of the changes in the surface salinity. These experiments allow a decomposition to investigate the specific role of the isopycnal migration from ΔT to the observed salinity changes on isopycnals.

1) LINEARITY OF THE CONTRIBUTION FROM THE SURFACE FORCINGS

To investigate the contribution of each surface forcing to the water mass changes, we look at changes in the salinity field on isopycnals. However, we first test whether ΔT and ΔS are additive to give the $\Delta T\Delta S$ results (Fig. 6). Subtracting the salinity trends of the combined experiment ($\Delta T\Delta S$) from the sum of the trends from the temperature (ΔT) and the salinity (ΔS) experiments ($\Delta T + \Delta S - \Delta T\Delta S$), we find only weak salinity trends on isopycnals (Figs. 6a–c). The correlation between the zonal average salinity trend in density for $\Delta T\Delta S$ and $\Delta T + \Delta S$ is 0.98 for the Atlantic Ocean, Indian Ocean, and global ocean and 0.99 for the Pacific Ocean. The small residual trends correlate to those from the sum of ΔT and ΔS (Figs. 6d–f) and are much smaller than those in the individual runs. This suggests that, for the surface changes we impose, the salinity and temperature forcings act essentially independently when transmitted into the interior along isopycnals. This linearity assists in the understanding of the observed and modeled changes discussed in the next sections.

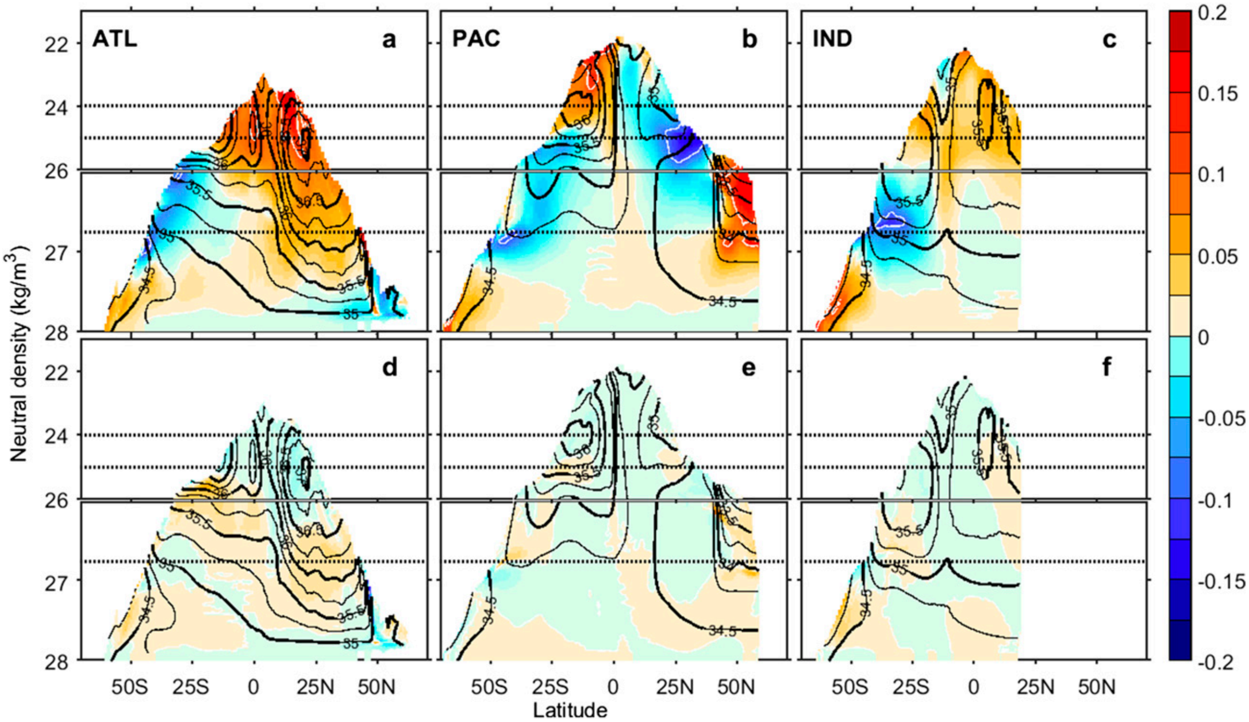

FIG. 6. (a)–(c) Zonally averaged salinity changes [PSS-78 (50 yr)$^{-1}$] on neutral density for the sum of ΔT and ΔS and (d)–(f) zonally averaged salinity trend on neutral density for the sum of ΔT and ΔS minus $\Delta T\Delta S$. The white contours are the salinity trend every 0.1PSS-78. The black contours are the mean salinity every 0.5 PSS-78 (thick lines) and 0.25 PSS-78 (thin lines). The dotted lines are the levels at which density surfaces are plotted on Fig. 8 (24, 25, and 26.75 kg m^{-3}).

2) ZONAL AVERAGES

In density space, the $\Delta T\Delta S$ accounts for nearly all the major observed water mass changes (Fig. 7). These include increases in subtropical salinity maxima, the freshening between this maxima and the Intermediate Water minima (AAIW and North Pacific Intermediate Water), and a salinity increase in waters denser than AAIW around Antarctica. These common changes across basins are all qualitatively reproduced in the combined $\Delta T\Delta S$ simulation.

In the Atlantic Ocean, ΔT has a negative salinity trend of approximately -0.2 (50 yr)$^{-1}$ centered around 30°S and at densities between 25 and 26 kg m^{-3} (see Fig. 7c). In ΔS, there is a positive salinity trend of approximately 0.2 (50 yr)$^{-1}$ centered around 20°S and at 25 kg m^{-3} (Fig. 7d). These two competing trends cancel each other out to reproduce the transition between positive and negative trend at 25.5 kg m^{-3} between 20° and 40°S as seen in the observations. The negative trend in the observations at densities between 25 and 26.5 kg m^{-3} is reproduced with ΔT and the positive trend in the observations between 24 and 25 kg m^{-3} with ΔS. This is one of several examples where ΔT and ΔS drive canceling trends and only their sum reproduces the observations.

In the North Pacific, near the equator at the densities lighter than 24 kg m^{-3}, ΔS has a negative salinity trend while ΔT has a positive trend (see Figs. 7g,h). These largely cancel to leave a small negative trend in $\Delta T\Delta S$. The observations present a positive trend for this area. The surface freshening imposed in the model in the midlatitude North Pacific is stronger and covers a larger area than observed for the same region, and the model's North Pacific salinity maxima is smaller (Figs. 1b,d). The increase in salinity due to the outcrop migration into the salinity maxima is thus limited. At the same time, ΔS induces a freshening stronger than in the observations. These two biases combine to give a net freshening in the model while the observations have an increase in salinity.

In the Indian Ocean, the increase in salinity at densities lower than $\sigma \approx 24$ kg m^{-3} is reproduced in ΔT (Figs. 7i,k). It is partially canceled by a freshening in ΔS (Figs. 7j,l). The region of salinity increase in the observations of the Indian Ocean is not as salty in our experiment's idealized surface salinity field (Figs. 1b,d). This can explain the weaker salinity increase in $\Delta T\Delta S$.

However, some observed changes are not simulated accurately through these simple experiments. The freshening originating along $\sigma \approx 27$ kg m^{-3} in the South

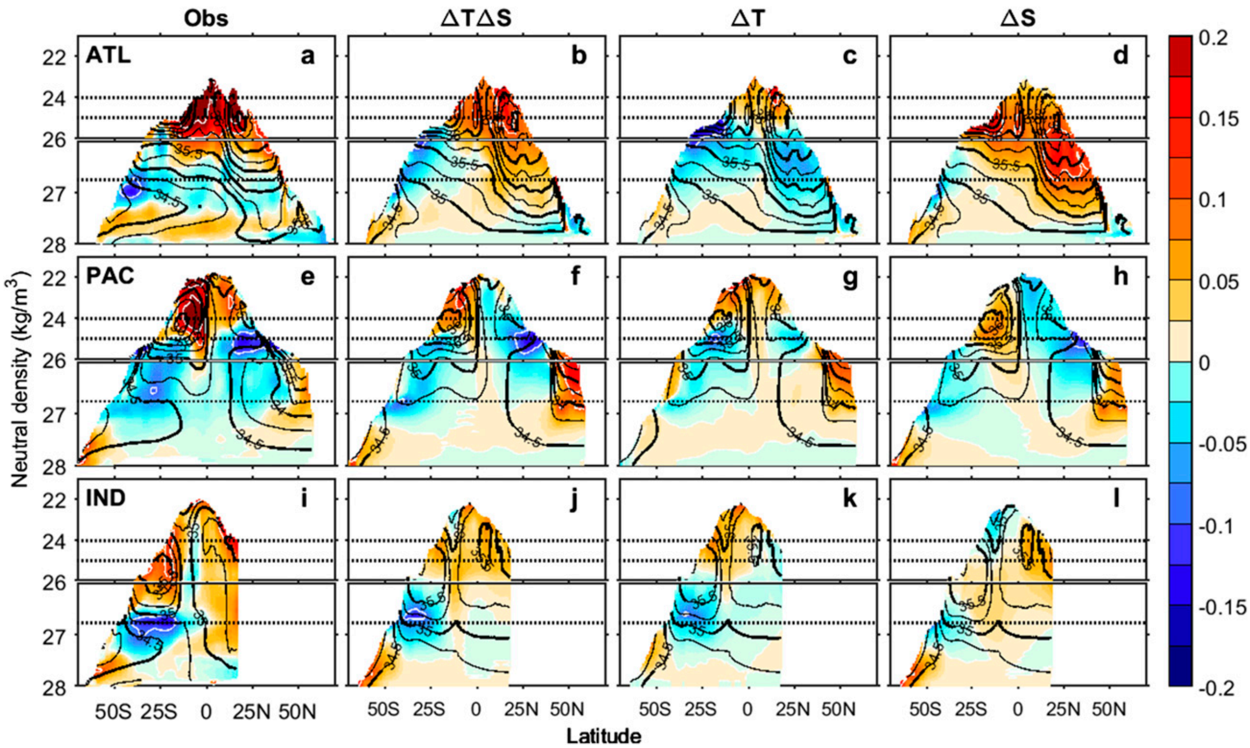

FIG. 7. Zonally averaged salinity changes [PSS-78 $(50\,\mathrm{yr})^{-1}$] on neutral density in the (a)–(d) Atlantic, (e)–(h) Pacific, and (i)–(l) Indian Oceans. (left to right) Observations, $\Delta T\Delta S$, ΔT, and ΔS. The white contours are the salinity trend every 0.1 PSS-78. The black contours are the mean salinity every 0.5 PSS-78 (thick lines) and 0.25 PSS-78 (thin lines). The dotted lines mark where σ = 24, 25, and 26.75 kg m^{-3}, which we examine in more detail.

Atlantic does not penetrate far enough northward. This is likely due to the weak northward penetration of AAIW in the model as seen in the mean contours (Fig. 7). The model does not reproduce the propagation of the Mediterranean Sea outflow salinity increase through the Atlantic at $\sigma \approx 27.7\,\mathrm{kg\,m^{-3}}$; it is at lesser densities of σ values of roughly 26.75 to 27 kg m^{-3} in the model (Figs. 7a,b).

The salinity increase near the equator in the North Pacific is not reproduced in the experiment. The surface freshening imposed at the surface in the model in the midlatitude North Pacific is stronger and over a larger area than observed for the same region (Figs. 1b,d). This amplifies the freshening from ΔS and negates the positive trend from ΔT. The increase in salinity in the north Indian Ocean is not as prevalent and does not penetrate as deep, but again the model is missing the denser Red Sea water overflow (Figs. 7i,j). The freshening of the ITF plume is not well reproduced in the model. The freshening, like the mean ITF, is mixed and less defined than observations (Figs. 7i,j).

Densities heavier than $\sigma \approx 27\,\mathrm{kg\,m^{-3}}$ are less well ventilated than observed. The ventilation at these densities happens largely via the North Atlantic Deep Water and the Antarctic Bottom Water formation. Observed salinity increases in these densities are associated with Upper Circumpolar Deep Water (UCDW) in the Southern Hemisphere high latitudes. The salinity increase in the UCDW throughout the Southern Ocean is reproduced in $\Delta T\Delta S$ (Figs. 7b,f,j). The increase in salinity in the Pacific and Atlantic UCDW is reproduced mainly through ΔS, although with some small contribution from ΔT (Fig. 7). As we do not warm the ocean surface south of 55°S with ΔT and $\Delta T\Delta S$, this limits the induced changes and helps to explain why the corresponding salinity trend in $\Delta T\Delta S$ is smaller than in the observations.

Overall most key features are reproduced through either ΔT or ΔS and together in $\Delta T\Delta S$. Specific features of salinity changes are reproduced mainly by ΔS and complemented through ΔT, or vice versa or through equal contribution. In some instances, a feature produced through the surface salinity change is canceled out by changes produced through ΔT. In these cases, in ΔT ΔS, and in the observation, there is little salinity change even though each experiment individually produces salinity trends. This reflects the importance of considering the shifts in the isopycnals through changes in temperature when assessing salinity trends in the ocean interior.

3) Correlation of simulated salinity change with observations

We explore the zonally averaged changes in density between each experiment and the observations via spatial correlations (Table 2). The density level at which the salinity changes occur in the experiments varies from the observations as the model does not represent the water masses necessarily in the same density classes. The differences in the density classes limit the interpretation of the direct correlation between the modeled and observed salinity changes. Nonetheless, the spatial correlation gives an idea of how well the salinity changes are reproduced within these idealized simple experiments, keeping in mind the differences in water mass classification in the interpretation.

The correlations of $\Delta T\Delta S$ with the observations are high in all three ocean basins, which indicates that the major patterns of water mass salinity changes are reproduced. In every basin, the correlation of $\Delta T\Delta S$ with the observed changes is higher than either ΔS or ΔT. The Atlantic pattern has a bigger contribution from ΔS, and the Pacific and Indian patterns have a stronger contribution from ΔT. The Atlantic has a stronger surface salinity increase (Figs. 1b,d), which explains the stronger contribution from the salinity changes. Both ΔT and ΔS have globally similar correlation with $\Delta T\Delta S$. The salinity changes in ΔT and ΔS anticorrelate, particularly in the Atlantic, where the effect of the surface temperature change and salinity change at the surface have an opposite effect on the subsurface salinity change.

4) Regional distribution of salinity change when $\sigma = 24\,\mathrm{kg\,m^{-3}}$: Upper thermocline

Each of the maps on Fig. 8 illustrates regionally, with varying intensity, the changes in salinity from the poleward migration of isopycnals (ΔT) and the salinity amplification (ΔS). Patterns on these density surfaces enlighten the surface to interior connections along the isopycnals.

When $\sigma = 24\,\mathrm{kg\,m^{-3}}$ (Fig. 8a), the observations generally increase in each basin. In $\Delta T\Delta S$, this increase in salinity is reproduced with a smaller intensity in the Atlantic, South Pacific, and Indian Oceans (Fig. 8b). The positive salinity trends in ΔT reflect the poleward migration of this density outcrop through the mean salinity field from lower tropical salinities toward the subtropical salinity maxima (Figs. 2a and 8c). Salinity changes in ΔS reflect the subduction of the surface salinity pattern amplification (Fig. 8d). The regions of

TABLE 2. Spatial correlation coefficients for zonally averaged salinity change patterns in density space (see Fig. 7). The first column has the correlation between each experiment and observations and the second and third column the correlation between each experiment. The control experiment has been subtracted prior to calculation in all cases.

		Observations	ΔS experiment	ΔT experiment
$\Delta T\Delta S$ experiment	Atlantic	0.72	0.60	0.49
	Pacific	0.64	0.68	0.69
	Indian	0.59	0.53	0.73
	Global	0.81	0.53	0.66
ΔT experiment	Atlantic	0.24	−0.39	
	Pacific	0.49	−0.05	
	Indian	0.46	−0.17	
	Global	0.53	−0.25	
ΔS experiment	Atlantic	0.54		
	Pacific	0.37		
	Indian	0.28		
	Global	0.44		

increased surface salinity in ΔS are subducted in the South Pacific, north-northwest Indian, and Atlantic Oceans. Similarly, regions of surface freshening in ΔS correspond to freshening on the isopycnal as in the south Indian and South Pacific Oceans.

The whole Atlantic Ocean has a positive salinity trend where $\sigma = 24\,\mathrm{kg\,m^{-3}}$ (Fig. 8a). This is reproduced in both ΔT and ΔS; they add in $\Delta T\Delta S$ to render a salinity increase closer to the observations, although at a lower intensity (Figs. 8a–d). The surface salinity forcing in the Atlantic in our experiments is less than in the observations in the tropics, and so is the warming (Figs. 1a–d). This explains the smaller increase in salinity in $\Delta T\Delta S$.

In the South Pacific Ocean, the observations indicate an increase in salinity (Fig. 8a). The salinity increase comes from ΔS and is slightly amplified with ΔT (Figs. 8c,d). The salinity increase in ΔS starts on the eastern side of the South Pacific at the location of increased surface salinity (Fig. 1b). The salinity increase in ΔT originates on the western side, where the outcrops migrate to a higher salinity (Fig. 4a). For $\Delta T\Delta S$, the magnitude of the pattern is reproduced but with a magnitude about half of that in the observations, which reflects the smaller salinity increase in the tropics of the South Pacific with ΔS (Figs. 1b,d).

In the North Pacific, $\Delta T\Delta S$ produces a freshening, opposite to the salinity increase seen in the observations (Figs. 8e,f). There is a slight salinity increase in ΔT, but this salinity increase is canceled in $\Delta T\Delta S$ by a stronger freshening in ΔS. This failure to reproduce the observations is a result of a weaker and smaller region of high surface salinity forcing in the model around 20°N where this isopycnal outcrops (Figs. 1b,d). Also, the increase in

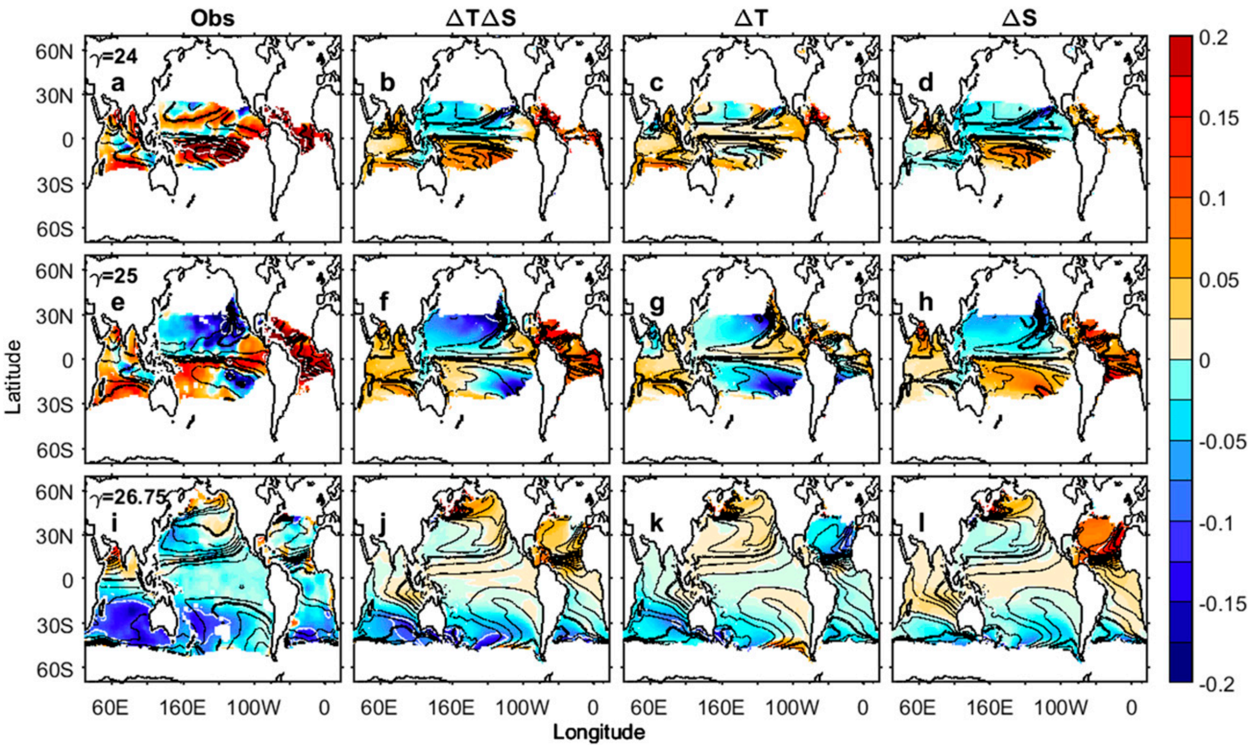

FIG. 8. Salinity changes [PSS-78 $(50\,\mathrm{yr})^{-1}$] on neutral-density surfaces at (a)–(d) 24, (e)–(h) 25, and (i)–(l) 26.75 kg m^{-3}. (left to right) Observations, the temperature increase experiment, the salinity pattern increase experiment, and both increased. The black contours are the mean salinity every 0.5 PSS-78 (thick lines) and 0.25 PSS-78 (thin lines).

salinity with ΔT is smaller because the outcrops do not migrate across as strong a salinity gradient as compared to the observations (Figs. 4a,d).

5) Regional distribution when $\sigma = 25\,\mathrm{kg\,m^{-3}}$: Midthermocline

The $\sigma = 25\,\mathrm{kg\,m^{-3}}$ surface slices through the ventilated gyre in each basin (except for the north Indian) and outcrops in particularly high meridional salinity gradients; it is thus affected by the salinity amplification at midlatitudes. This can be seen in Fig. 7 as the $\sigma = 25\,\mathrm{kg\,m^{-3}}$ density surface reaches regions of dense mean salinity contours near the surface. In the observations, the surface where $\sigma = 25\,\mathrm{kg\,m^{-3}}$ has decreased in salinity in the North Pacific, in the eastern South Pacific, and in the ITF tongue (Fig. 8e). In contrast, the salinity increases in the western South Pacific, the equatorial eastern Pacific, and the Atlantic Oceans, as well as most of the Indian Ocean. These features are well reproduced with $\Delta T\Delta S$, though with a reduced amplitude (Fig. 8f). The freshening in the ITF is not reproduced, likely because the ITF tongue is very weak in the model as visible in the mean contours (Fig. 8f), and as a result the freshening in the western equatorial Pacific is not advected to the Indian Ocean. The salinity trends in ΔT also reflect the migration of the outcrops through the mean surface salinity field (Fig. 8g). The outcrops migrate away from a surface salinity maximum to lower salinities driving the freshening along subduction pathways in the North and eastern South Pacific.

In the Atlantic Ocean, the salinity increase is reproduced with ΔS. It reflects the subduction of the increased surface salinity (Fig. 8h). There is a negative trend in the South Atlantic with ΔT attenuating the salinity increase from ΔS (Fig. 8g). In ΔT, the outcrop migrates from the salinity maxima toward lower salinity at this location (Fig. 4a). The salinity gradient is not as pronounced in the observations as in the model at this location (Fig. 4). This explains the salinity increase being stronger in the observations in the South Atlantic.

In the South Pacific, there is a generalized freshening trend in ΔT (Fig. 8g). This reflects the poleward migration of the outcrop toward lower salinities (Fig. 4a). This is negated on the western side by the positive trend in ΔS (Fig. 8h). At this location, the surface salinity increases with ΔS, so waters of higher salinity are being subducted (Fig. 1b). The combination of both reproduces in $\Delta T\Delta S$ the observed transition between a negative trend on the eastern South Pacific and a positive trend in the western South Pacific (Figs. 8e,f). The salinity increase in ΔS and decrease in ΔT both stem from the eastern side of the South Pacific where the mean salinity maxima occur, and thus this is a sensitive region for salinity change through outcrop migration and subduction.

The North Pacific has a strong freshening trend in the observations (Fig. 8e). The freshening is reproduced in $\Delta T\Delta S$; it originates from ΔT and is amplified by ΔS (Figs. 8g,h). In $\Delta T\Delta S$, the freshening is accurately reproduced in amplitude and extent (Fig. 8f). In ΔT, the outcrops migrate from the North Pacific salinity maxima northward to lower salinities, which produce a freshening on the isopycnal. In ΔS, the freshening reflects the subduction of the small freshening in the North Pacific where the outcrop reaches the surface. These two effects act together to reproduce the total strong observed freshening.

The increase in salinity in the eastern equatorial Pacific is reproduced in ΔT (Figs. 8e–g). This is a region of high surface salinity gradient. With ΔT, the outcrops migrate toward regions of higher surface salinity, which drives an increase in salinity along the isopycnal.

Most of the Indian Ocean increases in salinity where $\sigma = 25\,\mathrm{kg\,m^{-3}}$ in the observations, except for the ITF (Fig. 8e). The ITF is weaker in the model, and thus its freshening is not reproduced in $\Delta T\Delta S$ (Fig. 8f). However, the rest of the salinity increase in the Indian Ocean is reproduced at lower intensity. In the south Indian Ocean, the increase in salinity is mainly reproduced in ΔT (Fig. 8g). The outcrop migrates southward toward the salinity maxima—hence the increase in salinity (Fig. 4a). However, in our experiment, this isopycnal outcrops slightly farther north than in the observations, in a region of smaller salinity gradient. This explains the smaller salinity increase in the south Indian Ocean. In the north Indian Ocean, the increase in salinity is reproduced entirely with ΔS (Fig. 8h). This increase in salinity is led by the Red Sea and Persian Gulf overflow and depends on surface changes in salinity in these marginal seas.

6) Regional distribution of salinity change when $\sigma = 26.75\,\mathrm{kg\,m^{-3}}$: Lower thermocline

The $\sigma = 26.75\,\mathrm{kg\,m^{-3}}$ surface is dominated by the propagation of the SAMW in the Southern Hemisphere (Figs. 7a,e,i and 8i). In the Northern Hemisphere, the only ocean in which this density level reaches the surface is the Atlantic, and it intersects the inflow of saline Mediterranean waters in the model, which spread at a lower density than observed (Fig. 8j). The propagation of the salinity increase originates from the Mediterranean Sea in the North Atlantic and is reproduced in $\Delta T\Delta S$, although it penetrates to lower densities than in the observations (Figs. 7a,b). The Mediterranean Sea did become saltier in the time frame of the observations (Potter and Lozier 2004) but not as much as in our idealized experiment, thus explaining the saltier nature of the Mediterranean Sea saline tongue in our experiment.

Across the Southern Ocean, the SAMW is freshening in all basins of the observations (Fig. 8i). This freshening is reproduced in $\Delta T\Delta S$, although it does not propagate as far northward. This signal partly originates from ΔS and is amplified with ΔT, except at the eastern South Pacific (Figs. 8k,l). At these latitudes, salinity has as much of a role on the migration of the outcrops as temperature does because of the lower temperature of the water. The strength of the observed freshening is not reproduced in these experiments. The penetration of the SAMW and AAIW is weaker in the model than in reality because of mixing that is too large, which likely explains why the salinity anomaly is not transferred to the subsurface to the same extent as observed.

The North Atlantic increases in salinity in $\Delta T\Delta S$ (Fig. 8j), which is not the case in the observations (Fig. 8i). This increase comes from ΔS and is slightly reduced by ΔT. The modeled salinity increase comes from the diffusion of the Mediterranean overflow at a lower density than in the observations. The freshening in ΔT comes from the poleward migration of the outcrops from the tropical North Atlantic surface salinity maximum toward lower salinities. In the observations there is a slight salinity change reflecting this poleward migration of the outcrops.

When $\sigma = 26.75\,\mathrm{kg\,m^{-3}}$, the subpolar North Pacific has a small positive salinity trend in the observations (Fig. 8i). This increase in salinity is stronger in $\Delta T\Delta S$ (Fig. 8j) and comes from a combination of both ΔT and ΔS (Figs. 8k,l). The decreased surface salinity and increased temperature in the western North Pacific both increase buoyancy and thus reduce convection (Figs. 1a,c). This stops the low-salinity water entering the ocean and leads to the observed increase in salinity. When both experiments are combined, the total positive trend is about 50% larger than observed. Since ΔS decreases the surface salinity more than observed in the subpolar North Pacific and at these latitudes ΔS impacts more significantly on density changes, $\Delta T\Delta S$ has a higher increase in salinity than in the observations.

The north Indian Ocean becomes saltier in the observations (Fig. 8i). The increase in salinity is not reproduced in $\Delta T\Delta S$ (Fig. 8j). This salinity increase originates from the overflow from the Red Sea and Persian Gulf. The model does not reproduce the overflow at the same density depth as seen in the mean salinity contours and, similar to the Mediterranean water, precludes a faithful simulation of change.

The observed salinity changes in the ocean interior are overall reproduced by $\Delta T\Delta S$. However, the salinity changes in $\Delta T\Delta S$ are often of smaller amplitude than observed. This is mainly due to discrepancies in the modeled idealized surface temperature and salinity change compared with the observed surface changes. The salinity changes on density surfaces in $\Delta T\Delta S$ require both the ΔT and ΔS experiments to be comparable with the observations. Both the poleward isopycnal migration due to surface warming and the amplification of the surface salinity pattern contribute equally to reproduce the observed subsurface salinity anomalies. In the Atlantic, ΔS contributes more to the total salinity changes. There are stronger surface salinity changes in the Atlantic than any other basin, which is consistent with the stronger impact it has on the subsurface salinity changes. In the Pacific and Indian Ocean, ΔT contributes more to the subsurface salinity changes through poleward outcrop migration with the quasi-constant mean salinity field.

4. Discussion

We have found that the majority of subsurface water mass changes observed by Durack and Wijffels (2010) over the past 50 years can be explained by simple uniform ocean surface warming and salinity pattern amplification. These surface changes are transported into the ocean by a nearly constant general circulation and fixed winds. They act linearly to reproduce together the major water mass salinity changes with correlations between 0.59 and 0.81 when compared with observations.

Most of the salinity changes in the oceans' interior on depth surfaces are reproduced through an amplification of the surface salinity pattern with little contribution from the ocean warming signal. This suggests that these subsurface salinity changes are a good indicator of the water cycle amplification. However, both surface temperature increases and surface salinity pattern amplification are needed to explain the observed trends of water mass properties on density surfaces. Most key features of observed salinity trends patterns are reproduced in $\Delta T\Delta S$, which is well approximated by a linear combination of the salinity changes in ΔT and ΔS.

A roughly equal contribution of surface temperature increase and surface salinity pattern amplification is required to explain the observations on density surfaces. In some locations, ΔS and ΔT have opposing trends and in others they reinforce a change. Overall, the migration of isopycnal outcrops needs to be considered when assessing the subsurface changes in salinity. This conclusion could be extrapolated to other tracers when their changes over time are assessed on density surfaces. The effect of outcrop migration would also contribute to subsurface changes of tracers such as oxygen, carbon dioxide, or nutrients in density spaces.

In these idealized experiments, variations in surface temperature and salinity combine linearly to produce changes in salinity in the subsurface ocean. It is possible that the linearity of these contributions would not persist for stronger surface temperature warming and salinity pattern amplification that might occur in a more rapidly warming world, as feedbacks may perturb the circulation more strongly. This will likely involve wind changes, and thus a coupled modeling approach would be required.

Regions where the simulations of change agree less well with observations generally correspond with features not well modeled in the mean: AAIW, marginal sea overflows, and the ITF. These failures imply subgrid-scale processes that are not simulated at this resolution. There are also differences in the amplitude of salinity changes because of discrepancies between our idealized simulations and the more complex observed surface temperature and salinity changes. However, it is remarkable that many of the complex regional patterns of change in subsurface salinity can be simulated by such simple surface perturbations.

Acknowledgments. The work of V.L., S.E.W., J.A.C., and S.J.M. is supported by the Australian Government Department of Environment, the Bureau of Meteorology, and CSIRO through the Australian Climate Change Science Program. This research was undertaken with the assistance of resources provided at the NCI National Facility systems at the Australian National University through the National Computational Merit Allocation Scheme supported by the Australian government. The work of P.J.D. from Lawrence Livermore National Laboratory is a contribution to the U.S. Department of Energy, Office of Science, Climate and Environmental Sciences Division, Regional and Global Climate Modeling Program under Contract DE-AC52-07NA27344. The work of V.L. and N.L.B. from the Institute of Marine and Antarctic Studies is supported by the University of Tasmania and the Centre of Excellence for Climate System Science.

REFERENCES

Arakawa, A., and V. R. Lamb, 1977: Computational design and the basic dynamical processes of the UCLA general circulation model. *Methods Comput. Phys.*, **17**, 173–265.

Bi, D., and Coauthors, 2013: ACCESS-OM: The ocean and sea ice core of the ACCESS coupled model. *Aust. Meteor. Oceanogr. J.*, **63**, 213–232.

Bindoff, N. L., and T. J. McDougall, 1994: Diagnosing climate change and ocean ventilation using hydrographic data. *J. Phys.*

Oceanogr., **24**, 1137–1152, doi:10.1175/1520-0485(1994)024<1137:DCCAOV>2.0.CO;2.

Boyer, T. P., S. Levitus, J. I. Antonov, R. A. Locarnini, and H. E. Garcia, 2005: Linear trends in salinity for the World Ocean, 1955–1998. *Geophys. Res. Lett.*, **32**, L01604, doi:10.1029/2004GL021791.

Cravatte, S., T. Delcroix, D. Zhang, M. McPhaden, and J. Leloup, 2009: Observed freshening and warming of the western Pacific warm pool. *Climate Dyn.*, **33**, 565–589, doi:10.1007/s00382-009-0526-7.

Curry, R., B. Dickson, and I. Yashayaev, 2003: A change in the freshwater balance of the Atlantic Ocean over the past four decades. *Nature*, **426**, 826–829, doi:10.1038/nature02206.

Dickson, B., I. Yashayaev, J. Meincke, B. Turrell, S. Dye, and J. Holfort, 2002: Rapid freshening of the deep North Atlantic Ocean over the past four decades. *Nature*, **416**, 832–837, doi:10.1038/416832a.

Drijfhout, S., D. Marshall, and H. Dijkstra, 2013: Conceptual models of the wind-driven and thermohaline circulation. *Ocean Circulation and Climate: A 21st Century Perspective*, G. Siedler et al., Eds., International Geophysics Series, Vol. 103, Academic Press, 257–282.

Durack, P. J., and S. E. Wijffels, 2010: Fifty-year trends in global ocean salinities and their relationship to broadscale warming. *J. Climate*, **23**, 4342–4362, doi:10.1175/2010JCLI3377.1.

——, ——, and R. J. Matear, 2012: Ocean salinities reveal strong global water cycle intensification during 1950 to 2000. *Science*, **336**, 455–458, doi:10.1126/science.1212222.

——, ——, and T. P. Boyer, 2013: Long-term salinity changes and implications for the global water cycle. *Ocean Circulation and Climate: A 21st Century Perspective*, G. Siedler et al., Eds., International Geophysics Series, Vol. 103, Academic Press, 727–757.

Freeland, H., K. Denman, C. S. Wong, F. Whitney, and R. Jacques, 1997: Evidence of change in the winter mixed layer in the northeast Pacific Ocean. *Deep-Sea Res. I*, **44**, 2117–2129, doi:10.1016/S0967-0637(97)00083-6.

Gordon, A. L., and C. F. Giulivi, 2008: Sea surface salinity trends over fifty years within the subtropical North Atlantic. *Oceanography*, **21**, 20–29, doi:10.5670/oceanog.2008.64.

Griffies, S. M., 2009: Elements of MOM4p1. GFDL Ocean Group Tech. Rep. 6, 444 pp.

——, and Coauthors, 2009: Coordinated Ocean-Ice Reference Experiments (COREs). *Ocean Modell.*, **26**, 1–46, doi:10.1016/j.ocemod.2008.08.007.

Hartmann, D. L., and Coauthors, 2013: Observations: Atmosphere and surface. *Climate Change 2013: The Physical Science Basis*, T. F. Stocker et al., Eds., Cambridge University Press, 159–254, doi:10.1017/CBO9781107415324.008.

Hegerl, G.C., and Coauthors, 2014: Challenges in quantifying changes in the global water cycle. *Bull. Amer. Meteor. Soc.*, **96**, 1097–1115, doi:10.1175/BAMS-D-13-00212.1.

Held, I. M., and B. J. Soden, 2006: Robust responses of the hydrological cycle to global warming. *J. Climate*, **19**, 5686–5699, doi:10.1175/JCLI3990.1.

Helm, K. P., N. L. Bindoff, and J. A. Church, 2010: Changes in the global hydrological-cycle inferred from ocean salinity. *Geophys. Res. Lett.*, **37**, L18701, doi:10.1029/2010GL044222.

Hosoda, S., T. Suga, N. Shikama, and K. Mizuno, 2009: Global surface layer salinity change detected by Argo and its implication for hydrological cycle intensification. *J. Oceanogr.*, **65**, 579–596, doi:10.1007/s10872-009-0049-1.

Hunke, E. C., and W. H. Lipscomb, 2010: CICE: The Los Alamos Sea Ice Model documentation and software user's manual. Los Alamos National Laboratory Tech. Rep. LA-CC-06-012, 76 pp. [Available online at http://csdms.colorado.edu/w/images/CICE_documentation_and_software_user's_manual.pdf.]

Johnson, G. C., and J. M. Lyman, 2007: Global oceans: Sea surface salinity [in "State of the Climate in 2006"]. *Bull. Amer. Meteor. Soc.*, **88** (6), S34–S35, doi:10.1175/BAMS-88-6-StateoftheClimate.

Kouketsu, S., M. Fukasawa, D. Sasano, Y. Kumamoto, T. Kawano, H. Uchida, and T. Doi, 2010: Changes in water properties around North Pacific Intermediate Water between the 1980s, 1990s and 2000s. *Deep-Sea Res. II*, **57**, 1177–1187, doi:10.1016/j.dsr2.2009.12.007.

Large, W. G., and S. G. Yeager, 2004: Diurnal to decadal global forcing for ocean and sea ice models: The data sets and flux climatologies. NCAR Tech. Note NCAR/TN-460+STR, 105 pp.

——, and ——, 2009: The global climatology of an interannually varying air–sea flux data set. *Climate Dyn.*, **33**, 341–364, doi:10.1007/s00382-008-0441-3.

Levitus, S., J. Antonov, and T. Boyer, 2005: Warming of the world ocean, 1995–2003. *Geophys. Res. Lett.*, **32**, L02604, doi:10.1029/2004GL021592.

——, and Coauthors, 2012: World ocean heat content and thermosteric sea level change (0–2000 m), 1955–2010. *Geophys. Res. Lett.*, **39**, L10603, doi:10.1029/2012GL051106.

Potter, R. A., and M. S. Lozier, 2004: On the warming and salinification of the Mediterranean outflow waters in the North Atlantic. *Geophys. Res. Lett.*, **31**, L01202, doi:10.1029/2003GL018161.

Rhein, M. S. R., and Coauthors, 2013: Observations: Ocean. *Climate Change 2013: The Physical Science Basis*, T. F. Stocker et al., Eds., Cambridge University Press, 255–315, doi:10.1017/CBO9781107415324.010.

Roemmich, D., and J. Gilson, 2009: The 2004–2008 mean and annual cycle of temperature, salinity, and steric height in the global ocean from the Argo program. *Prog. Oceanogr.*, **82**, 81–100, doi:10.1016/j.pocean.2009.03.004.

Schanze, J. J., R. W. Schmitt, and L. L. Yu, 2010: The global oceanic freshwater cycle: A state-of-the-art quantification. *J. Mar. Res.*, **68**, 569–595, doi:10.1357/002224010794657164.

Skliris, N., R. Marsh, S. A. Josey, S. A. Good, C. Liu, and R. P. Allan, 2014: Salinity changes in the World Ocean since 1950 in relation to changing surface freshwater fluxes. *Climate Dyn.*, **43**, 709–736, doi:10.1007/s00382-014-2131-7.

Sloyan, B. M., and I. V. Kamenkovitch, 2007: Simulation of subantarctic mode and Antarctic Intermediate Waters in climate models. *J. Climate*, **20**, 5061–5080, doi:10.1175/JCLI4295.1.

Terray, L., L. Corre, S. Cravatte, T. Delcroix, G. Reverdin, and A. Ribes, 2012: Near-surface salinity as nature's rain gauge to detect human influence on the tropical water cycle. *J. Climate*, **25**, 958–977, doi:10.1175/JCLI-D-10-05025.1.

Valcke, S., 2006: OASIS3 user guide: prism_2-5. PRISM Support Initiative CERFACS Rep. 3, 68 pp.

von Schuckmann, K., F. Gaillard, and P.-Y. Le Traon, 2009: Global hydrographic variability patterns during 2003–2008. *J. Geophys. Res.*, **114**, C09007, doi:10.1029/2008JC005237.

Wong, A. P. S., N. L. Bindoff, and J. A. Church, 1999: Large-scale freshening of intermediate waters in the Pacific and Indian Oceans. *Nature*, **400**, 440–443, doi:10.1038/22733.

——, ——, and ——, 2001: Freshwater and heat changes in the North and South Pacific Oceans between the 1960s and 1985–94. *J. Climate*, **14**, 1613–1633, doi:10.1175/1520-0442(2001)014<1613:FAHCIT>2.0.CO;2.